Folding of Apocytochrome *c* in Lipid Micelles: Formation of α-Helix Precedes Membrane Insertion†

Elzbieta A. Bryson,‡ Saffron E. Rankin,‡ Michael Carey,§ Anthony Watts,|| and Teresa J. T. Pinheiro*,‡

Department of Biological Sciences, University of Warwick, Gibbet Hill Road, Coventry CV4 7AL, United Kingdom, Applied Photophysics Ltd., 203/205 Kingston Road, Leatherhead, Surrey KT22 7PB, United Kingdom, and Department of Biochemistry, University of Oxford, South Parks Road, Oxford OX1 3QU, United Kingdom

Received January 20, 1999; Revised Manuscript Received May 17, 1999

ABSTRACT: Apocytochrome *c*, which in aqueous solution is largely unstructured, acquires a highly α-helical structure upon interaction with lipid. The α-helix content induced in apocytochrome *c* depends on the lipid system, and this folding process is driven by both electrostatic and hydrophobic lipid−protein interactions. The folding kinetic mechanism of apocytochrome *c* induced by zwitterionic micelles of lysophosphatidylcholine (L-PC), predominantly driven by hydrophobic lipid−protein interactions, was investigated by fluorescence stopped-flow measurements of Trp 59 and fluorescein−phosphatidylethanolamine- (FPE) labeled micelles, in combination with stopped-flow far-UV circular dichroism. It was found that formation of the α-helical structure of apocytochrome *c* precedes membrane insertion. The unfolded state in solution (U_W) binds to the micelle surface in a helical conformation (I_S) and is followed by insertion into the lipid micelle, i.e., formation of the final helical state H_L. Binding of apocytochrome *c* to the lipid micelle ($U_W \rightarrow I_S$) is concurrent with formation of a large fraction (75−100%, depending on lipid concentration) of the α-helical structure of the final lipid-inserted state H_L. The highly helical intermediate I_S is formed on the time scale of 3−12 ms, depending on lipid concentration, and inserts into the lipid micelle ($I_S \rightarrow H_L$) in the time range of ∼200 ms to >1 s, depending on lipid-to-protein ratio. The final lipid-inserted helical state H_L in L-PC micelles has an α-helix content ∼65% of that of cytochrome *c* in solution and has no compact stable tertiary structure as revealed by circular dichroism results.

Apocytochrome *c* (apocyt *c*)[1] is the precursor of the mitochondrial protein cytochrome *c*, which functions in the intermembrane space of mitochondria as an electron donor to the inner mitochondrial membrane protein cytochrome *c* oxidase. The precursor protein is encoded by nuclear DNA and synthesized on free cytoplasmic ribosomes without the heme group. Unlike most other mitochondrial precursor proteins, apocyt *c* is synthesized without a cleavable amino-terminal presequence, it does not require ATP or a membrane potential for translocation, and it does not use the mitochondrial translocation machinery (*1*). Instead, apocyt *c* can insert spontaneously and partially cross the outer mitochondrial membrane (*2*, *3*). After, or simultaneous with, translocation across the outer membrane, apocyt *c* is recognized by the enzyme cytochrome *c* heme lyase (CCHL), which attaches covalently the heme group to cysteines 14 and 17 (*4*, *5*). After heme binding, dissociation of holocytochrome *c* from CCHL is presumed to be triggered by folding of the polypeptide around the heme group into the native cyt *c* structure. Once the folded compact structure is formed, cyt *c* is confined to the intermembrane space and cannot cross back to the cytoplasm, unless the cell becomes apoptotic (*6*). Thus, the heme group in cyt *c* not only is essential for its function as an electron carrier and for its import pathway into mitochondria but also appears to play a crucial role in stabilizing the native fold of cyt *c*.

In vitro, when the heme group is removed from cyt *c*, the resulting apoprotein loses the secondary structure characteristic of the native holoprotein and shows the typical properties, as judged by circular dichroism and intrinsic viscosity, of a largely disordered structure in solution (*7*, *8*). A more recent study using peptide fragments of cyt *c* has shown that the unfolded state in solution contains a residual amount of α-helical structure consistent with formation of the C-terminal helix (*9*). However, the interaction of apocyt *c* with lipid (in the absence of heme) can generate a partially folded conformation with an α-helix content that resembles that of native cyt *c* (*10*−*12*). These studies had shown that the extent of lipid-induced secondary structure is dependent on lipid headgroup charges. Negatively charged phospholipid

† This work has been supported by the Royal Society and the Biotechnology and Biological Sciences Research Council, Grant 88/B09547 (T.J.T.P.). S.E.R. and E.A.B. were postdoctoral research fellows under the EC TMR network on Membrane Biogenesis FMRX-CT96-0004 (A.W. and T.J.T.P.). A.W. is a BBSRC Senior Research Fellow. T.J.T.P. is a Royal Society University Research Fellow.

* Correspondence should be addressed to this author: e-mail tp@dna.bio.warwick.ac.uk; telephone +44 1203 528 364; fax +44 1203 523 701.

‡ University of Warwick.

§ Applied Photophysics Ltd.

|| University of Oxford.

[1] Abbreviations: AEDANS, *N*-acetyl-*N*′-(5-sulfo-1-naphthyl)ethylenediamine; apocyt *c*, apocytochrome *c*; CD, circular dichroism; CMC, critical micelle concentration; cyt *c*, cytochrome *c*; FPE, fluorescein−phosphatidylethanolamine (*N*-[(5-fluoresceinyl)thiocarbamoyl]-1,2-dihexadecanoyl-*sn*-glycero-3-phosphoethanolamine); AEDANS, *N*-acetyl-*N*′-(5-sulfo-1-naphthyl)ethylenediamine; L-PC, lysophosphatidylcholine (1-myristoyl-2-hydroxy-*sn*-glycero-3-phosphocholine); L-PG, lysophosphatidylglycerol (1-myristoyl-2-hydroxy-*sn*-glycero-3-[phospho-*rac*-(1-glycerol)]).

10.1021/bi990119o CCC: $18.00
Published on Web 07/02/1999

vesicles induce more α-helical structure than zwitterionic vesicles. This suggested that negative charges in the lipid headgroup play an important role in the mechanism of lipid-induced folding of apocyt *c*. However, a more recent study shows that lysophospholipid micelles induce an even higher content of α-helical structure in apocyt *c* compared with phospholipid vesicles of identical lipid headgroup structures (*13*). The maximum α-helix content of apocyt *c* induced by negatively charged lysophospholipid micelles can reach nearly 100% of that of native cyt *c* in solution, as monitored by the intensity of the dichroic band at 222 nm. Furthermore, micelles of lysolipids with the same zwitterionic headgroup as phospholipid vesicles, which do not fold apocyt *c*, were able to induce an α-helical structure in apocyt *c* with ∼ 65% of the α-helix content of native cyt *c*. These results showed that hydrophobic lipid−protein interactions play a role in the lipid-induced folding process of apocyt *c*.

Despite cyt *c* being one of the most studied proteins over the last half-century, with a rich body of literature on its electron-transfer functions and evolutionary relationships between different organisms, in addition to a wealth of high-resolution three-dimensional structures, fundamental questions on the mechanism of cyt *c* biogenesis remain puzzling (*14*). Among them, and of special interest to us, are those unresolved questions concerning the translocation mechanism of apocyt *c* across the outer mitochondria membrane, the process of heme binding to the apoprotein, and ultimately the folding mechanism of cyt *c in vivo*. The folding of cyt *c* in solution has been well characterized using a wide range of biophysical approaches, which has led to the identification of various intermediates in the folding pathway of cyt *c* in solution (*15*−*17*). Stopped-flow measurements of Trp 59 fluorescence and time-resolved far-UV circular dichroism studies have shown evidence of a compact intermediate (I_C) with native-like helix content that accumulates during the first few milliseconds of refolding. This early intermediate lacks a near-UV CD band (*16*) and shows no significant amide protection (*15*), indicating that it is a very loosely folded state without persistent hydrogen bonds. More recent hydrogen exchange labeling results revealed small, but measurable protection (protection factors up to ∼7) in the three main α-helices in the burst intermediate formed within 2 ms of refolding (*18*). After this initial hydrophobic collapse, specific tertiary contacts are formed between the N- and C-terminal helices, resulting in a subsequent intermediate (I_{NC}) that accumulates in about 10 ms (*15*). The final rate-limiting step in folding at neutral pH involves dissociation of a non-native histidine ligand (0.1−1 s) followed by rapid completion of folding, including formation of the native Met 80 ligation (*17*). It is pertinent to investigate whether analogous folding intermediates are involved in the folding mechanism of apocyt *c* in lipid membranes, particular the early intermediates I_C and I_{NC}, which are not associated with heme ligation.

Since apocyt *c* is capable of refolding from its unfolded state in solution to a highly helical state in lipid membranes (in the absence of the heme group) and a direct interaction with the lipid membrane appears to be involved in the import pathway into mitochondria, it is tempting to postulate that the lipid-induced partially structured states of apocyt *c* might be involved in the *in vivo* folding mechanism of cyt *c*. Therefore, it is relevant to investigate the folding of apocyt *c* driven by lipid and examine whether lipid-associated states correspond to the folding intermediates identified in the folding mechanism of cyt *c* in solution. Here we describe the kinetic folding mechanism of apocyt *c* in zwitterionic lipid micelles, which is predominantly driven by hydrophobic lipid−protein interactions. We show that formation of the α-helical structure of apocyt *c* precedes membrane insertion. The unfolded state of apocyt *c* in solution (U_W) binds to the micelle surface in an extended conformation ($U_W \rightarrow I_S$) and is followed by lipid insertion ($I_S \rightarrow H_L$). The intermediate state I_S has about 75−100% (depending on lipid concentration) of the α-helix content of H_L. The final lipid-inserted helical state H_L in L-PC micelles has an α-helix content ∼65% of that of native cyt *c* in solution with no stable tertiary structure and is as compact as the unfolded state U_W.

EXPERIMENTAL PROCEDURES

Materials and Protein Purification. Lysophosphatidylcholine (1-myristoyl-2-hydroxy-*sn*-glycero-3-phosphocholine) was purchased from Avanti Polar Lipids, Inc. (Alabaster, AL). Cyt *c* from horse heart (Type VI, Sigma Chemical Co., St. Louis, MO), which comes contaminated with a variety of deamidated forms of the protein, was purified by ion-exchange chromatography on a Whatman CM-32 column and eluted with a step gradient from 65 to 80 mM phosphate buffer, pH 7.0 (*19*). The eluent containing the purified protein was dialyzed against cold distilled water (4 °C), lyophilized, and stored at −20 °C. Cyt *c* concentration was measured spectrophotometrically with a molar absorption coefficient of 29 500 M^{-1} cm^{-1} at 550 nm and pH 7.0 for the protein reduced with sodium dithionite (*20*). Apocyt *c* was prepared by chemically removing the heme group of horse heart cyt *c* as described by Fisher et al. (*8*). Protein concentration was determined with a molar absorption coefficient of 10 580 M^{-1} cm^{-1} at 277 nm (*7*). Apocyt *c* was renatured by a modified procedure of that described by Hennig and Neupert (*21*) as described previously (*13*).

L-PC Micelles. Aqueous solutions of lysophospholipid micelles were prepared by dissolving the desired amount of dried lipid in 10 mM phosphate buffer, pH 7.0, followed by sonication (30 min, at room temperature) in a water bath sonicator (Ultrawave U-400). A few representative lipid samples were checked by thin-layer chromatography after sonication of micelles. No degradation products were detected relative to the original source lipid. The critical micelle concentration (CMC) under our experimental conditions (10 mM phosphate buffer, pH 7.0, at 10 °C) of L-PC was found to be 40 μM (*13*). Micelle sizes of a few representative samples were determined by dynamic light scattering on a Dyna-Pro 801 dynamic light scattering instrument. L-PC micelles showed a hydrodynamic diameter range of 60−80 Å. By taking a value for the radius of a spherical micelle based on the total length of the hydrocarbon chain plus the polar headgroup and by assuming a cross-sectional area per lipid headgroup on the micelle surface of 69.5 $Å^2$ (*22*), it was calculated that each micelle contained on average 160 lysolipid molecules.

CD Spectra. Circular dichroism measurements were performed with a Jasco J-715 spectropolarimeter. CD spectra of the far-UV (185−260 nm) were recorded at 10 ± 0.2 °C in cells of 1 mm path length, while for the near-UV (250−

350 nm) 0.75 cm path length cells were used. Typically, a scanning rate of 100 nm/min, a time constant of 1 s, and a bandwidth of 1.0 nm were used. Spectral resolution was 0.5 or 1 nm, and 4−16 scans were averaged per spectrum. The corresponding appropriate backgrounds (buffer for protein solutions, or lipid alone at corresponding concentrations for lipid−protein samples) were subtracted from the final spectra.

Fluorescence Spectra. Fluorescence spectra of apocyt *c* and AEDANS-labeled apocyt *c* were obtained on a Perkin-Elmer luminescence spectrometer LS50. For Trp fluorescence measurements of apocyt *c* the excitation wavelength was 295 nm (4 nm bandwidth), and emission spectra were recorded with 4 nm band-pass. Spectra of AEDANS-labeled apocyt *c* were recorded over a wavelength region from 300 to 600 nm covering the emission spectral regions for Trp 59 and AEDANS groups in the protein, after excitation at 285 nm (band-pass 4 nm, for excitation and emission). All fluorescence spectra were recorded at 10 ± 0.2 °C.

Stopped-Flow Trp 59 Fluorescence Kinetics. Fluorescence kinetic measurements were performed on a MicroVolume stopped-flow reaction analyzer SX.18MV instrument (Applied Photophysics Ltd., Leatherhead, U.K.) equipped with a modified T mixer, designed by Applied Photophysics, and a 2 × 1 × 10 mm flow cell. A 150-W xenon arc lamp (Osram, Germany) and monochromator were used for excitation at 295 nm (4.2 nm bandwidth) along the 10-mm axis of the cell. Fluorescence emission was detected in the 2-mm direction using a high-pass glass filter with a 320-nm cutoff and an electronic filter with a time constant of 100 μs. The changes in fluorescence emission were monitored over variable time scales up to 100 s. The stopped-flow module and observation cell were thermostated at 10 ± 0.2 °C. Lipid-induced folding of apocyt *c* was initiated by rapid mixing equal volumes of protein with L-PC micelles, both in 10 mM phosphate buffer, pH 7.0. The nominal dead time of the stopped-flow apparatus was 1.7 ± 0.2 ms. One thousand data points were acquired on a logarithmic time base with digital oversampling. For each kinetic measurement 4−16 traces were averaged and analyzed by the use of the Applied Photophysics software and IGOR (Wavemetrics, Lake Oswego, OR). Kinetic parameters were obtained by nonlinear least-squares analysis with a minimum number of exponential phases.

Stopped-Flow CD Kinetics. Far-UV CD kinetic measurements were performed on a π*-180 CDF spectrometer from Applied Photophysics Ltd. (Leatherhead, U.K.). The instrument was used in stopped-flow CD mode with the orientation of the flow cell (20 μL volume) set for a 2 mm optical path. The CD probe beam was generated from a 75 W mercury−xenon light via a twin grating monochromator and a 50 kHz photoelastic modulator. Measurements were made at 225 nm with a 4 nm spectral bandwidth. The stopped-flow module and observation cell were thermostated at 10 ± 0.2 °C. Lipid-induced folding of apocyt *c* was initiated by rapid mixing of equal volumes of protein solution (final concentration 10 μM) with lipid solutions at various concentrations, both in 10 mM phosphate buffer, pH 7.0. The deadtime of these measurements was 1.7 ± 0.3 ms. One thousand data points were acquired on a logarithmic time base with digital oversampling. For each kinetic measurement 32 traces were averaged and analyzed by use of the Applied Photophysics Pro-K analysis software and IGOR (Wavemetrics, Lake Oswego, OR). Kinetic parameters were obtained by nonlinear least-squares analysis with a minimum number of exponential phases.

FPE Labeling and Kinetic Measurements. Incorporation of FPE into L-PC micelles was achieved by the method originally described for labeling the outer leaflet of vesicles (*29*). Briefly, the FPE probe was added to L-PC micelles from a stock ethanolic solution of 5 mg/mL and incubated for 1 h at 20 °C. Free FPE was removed from the labeled micelles by gel filtration on Sephadex PD10 columns (Pharmacia) equilibrated with 10 mM phosphate buffer, pH 7.0. The degree of incorporation was estimated by absorbance measurements at 490 nm before and after separation on the PD10 column. Typically, the molar ratio of incorporated FPE to L-PC was about 1:240, which corresponds to approximately one FPE molecule per micelle. Stopped-flow FPE fluorescence measurements were performed on the SX.18MV stopped-flow instrument (Applied Photophysics Ltd., Leatherhead, U.K.) described above for the Trp 59 fluorescence kinetics. A monochromator was used for the excitation at 490 nm (4 nm bandwidth) and a high-pass glass filter with a cutoff at 515 nm was used for detection of fluorescence emission. A thousand data points were collected on a logarithmic time base with digital oversampling and an electronic filter with a time constant of 100 μs over a time scale up to 100 s. Measurements were performed at 10 ± 0.2 °C by mixing equal volumes of protein solution with labeled lipid micelles, both in 10 mM phosphate buffer, pH 7.0. Typically, for each kinetic measurement four traces were averaged and analyzed as described above. Kinetic parameters were obtained by nonlinear least-squares analysis with a minimum number of exponential phases.

RESULTS

Structural Changes in Apocyt c Induced by L-PC Micelles. In contrast with cyt *c*, which in aqueous solution has a compact well-defined structure, the heme-free precursor protein apocyt *c* is a disordered structure in solution, as revealed by the far-UV circular dichroism spectrum (Figure 1). However, the interaction of apocyt *c* with lipid membranes and detergent micelles can lead to a highly helical state, which can resemble that of native cyt *c* in solution (*10*−*12*). We have recently examined the extent of folding of apocyt *c* induced by various lipid systems, including phospholipid vesicles and lysophospholipid micelles (*13*). We have shown that the level of secondary structure induced in the protein is determined by two main driving forces: (a) electrostatic interactions between negatively charged lipid headgroups and positively charged residues in the polypeptide chain and (b) hydrophobic interactions between nonpolar residues in the protein and the hydrophobic core of the lipid membrane or micelle. In contrast with zwitterionic vesicles in the presence of which apocyt *c* remains a random coil, binding to zwitterionic L-PC micelles shows the typical features characteristic of proteins containing mainly α-helical structure (Figure 1). These spectral changes indicate that, upon interaction with L-PC, apocyt *c* undergoes a conformational transition from its random coil state in solution to an α-helical structure. The α-helix content of apocyt *c* increased with increasing concentrations of L-PC below 1 mM and remained constant for concentrations above 1 mM lipid (Figure 1, inset). This maximum value of α-helix

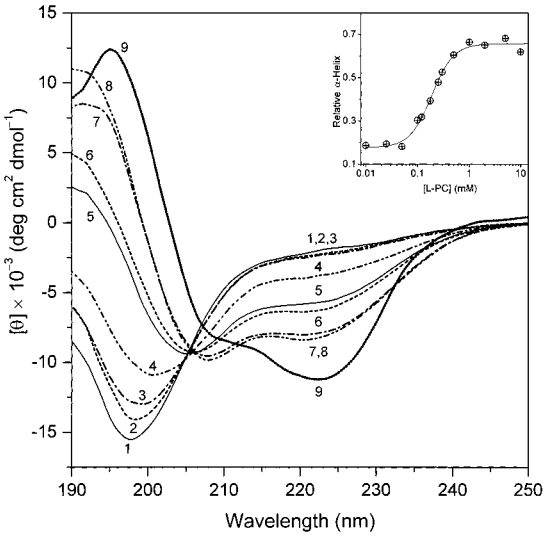

FIGURE 1: Far-UV circular dichroism spectra of apocyt *c* in solution (1) and in the presence of various concentrations of L-PC: 10 μM (2); 50 μM (3); 120 μM (4); 250 μM (5); 500 μM (6); 2 mM (7); and 5 mM (8), in comparison with the far-UV CD spectrum of cyt *c* in solution (9). Protein concentration was 10 μM. Proteins and lipid were both in 10 mM phosphate buffer, pH 7.0. Spectra are an average of eight scans, recorded at 10 °C in cells of 1 mm path length. Inset: α-Helix level induced in apocyt *c* as a function of L-PC concentration monitored by the ellipticity at 222 nm relative to that of cyt *c* in solution. Line is for guidance only and has no theoretical significance.

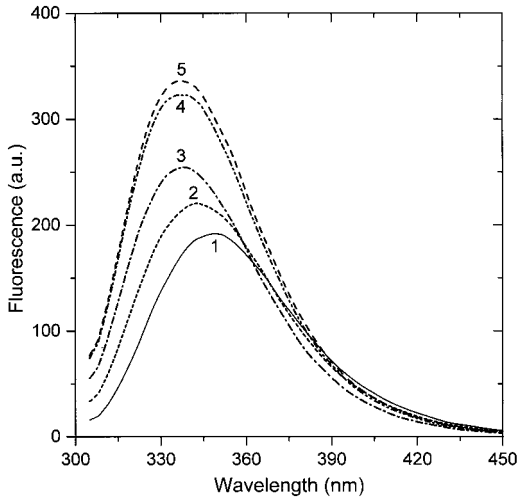

FIGURE 2: Fluorescence emission spectra of apocyt *c* in aqueous solution (1) and with various concentrations of L-PC: 150 μM (2); 500 μM (3); 1 mM (4); and 2 mM (5). Protein concentration was 10 μM, and protein and lipid micelles were both in 10 mM phosphate buffer, pH 7.0. Spectra were recorded at 10 °C, with an excitation wavelength at 295 nm.

represents about 65% of that of cyt *c* in solution, as monitored by the intensity of the 222 nm dichroic band. The CD spectra in Figure 1 show an isodichroic point for apocyt *c* at various L-PC concentrations, which is consistent with a two-state transition. However, the spectrum of holocyt *c* does not pass through this point, which could be due to structural differences between the apo and holo proteins (contributions from nonhelical regions of the native protein that are probably unstructured in the micelle-bound form of apocyt *c*) or contributions of the heme to the far-UV CD spectrum of cyt *c*.

The single tryptophan residue (Trp 59) in apocyt *c* is a useful probe to monitor the interaction of apocyt *c* with lipid membranes (*13*). We have examined the fluorescence changes of Trp 59 upon mixing with various concentrations of L-PC from below to above the CMC. Binding of apocyt *c* to L-PC micelles results in a significant increase in the fluorescence emission of Trp 59 and a blue shift in the wavelength of maximum fluorescence intensity (λ_{max}) up to 11 nm (Figure 2). The changes in the blue shift of λ_{max} as a function of lipid concentration have been shown to correlate well with the changes in α-helical structure and coincide with the formation of micelles (*13*). This shows that (a) apocyt *c* interacts preferably with L-PC micelles rather than with monomeric molecules of L-PC and (b) Trp 59 fluorescence changes can report on the folding of apocyt *c* in lipid micelles.

Trp 59 Stopped-Flow Folding Kinetics of Apocyt c in Lipid Micelles. The use of fluorescence intensity changes of Trp 59 to monitor the folding kinetics has been previously demonstrated for the folding of cyt *c* in solution (*16, 17, 26, 27*), unfolding of cyt *c* induced by the interaction with lipid vesicles (*28*), and folding of apocyt *c* upon binding to negatively charged lysolipid micelles (*25*). In the current study, we have investigated the time dependence of the Trp 59 fluorescence of apocyt *c* resulting from the interaction with the zwitterionic lysolipid, L-PC, using stopped-flow experiments. The changes in fluorescence emission (detected above 310 nm) relative to the initial fluorescence of unfolded apocyt *c* in buffer solution were monitored over a time range up to 100 s after rapid mixing with lipid at various protein and lipid concentrations (>CMC). Representative kinetic traces are shown in Figure 3A, where the changes in fluorescence are plotted on a logarithmic time scale. Stopped-flow control experiments in which L-PC at various concentrations (0.05−5 mM) was mixed with buffer in the absence of protein revealed a small lipid scattering background, which increased with lipid concentration. For the highest lipid concentration (5 mM) the deviation from buffer alone was ∼ 20% of the overall fluorescence change of apocyt *c* induced by the interaction with lipid. Lipid backgrounds were subtracted from the corresponding kinetic traces. Figure 3B presents the first 10 ms of the kinetics on a linear time scale to show that all traces extrapolate to the initial fluorescence level of unfolded apocyt *c* in solution (1.00 ± 2.5%), which indicates that in these folding measurements there is no burst phase (i.e., no missing amplitude). A summary of rates and amplitudes for the fluorescence-detected kinetics at various lipid and protein concentrations is presented in Tables 1 and 2.

The fluorescence-detected stopped-flow results show three distinct kinetic events: (A) A fast phase on the 10 ms time scale has a rate and amplitude strongly dependent on lipid concentration (k_1 = 80−380 s^{-1} for [L-PC] = 100−5000 μM; Table 1). The amplitude associated with this phase carries a large fraction of the total fluorescence change (34% for 200 μM L-PC increasing to ∼100% for [L-PC] ≥ 2 mM). (B) An intermediate phase (20−150 ms) has a rate dependent on lipid concentration (Table 1) and independent of protein concentration (Table 2). The amplitude associated with this phase is independent of protein concentration (Table 2) and goes through a maximum at intermediate lipid concentrations ([L-PC] ≈ 1 mM, see Table 1) where it reaches ∼ 40% of

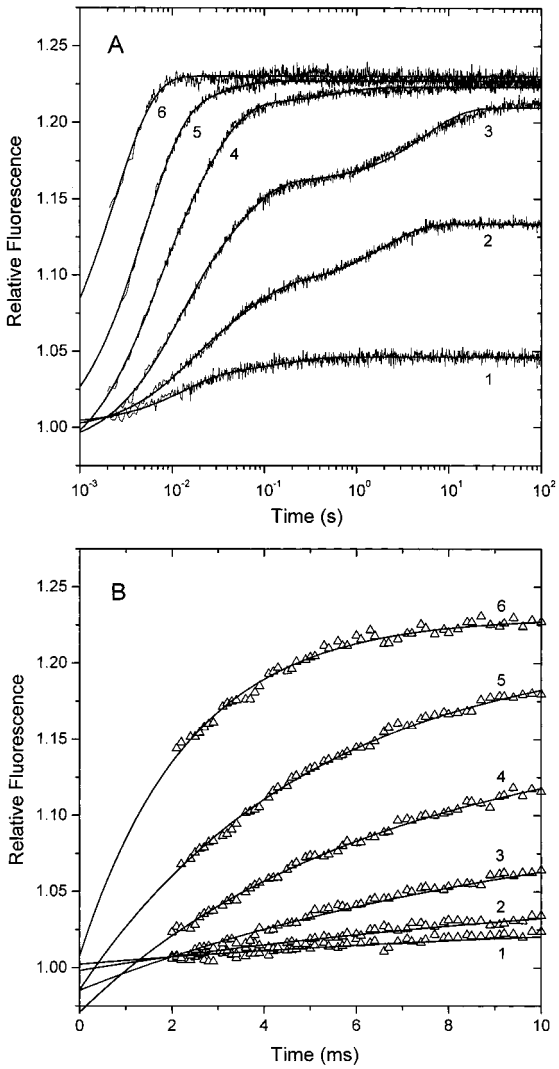

FIGURE 3: Representative tryptophan fluorescence kinetics for the interaction of apocyt *c* with L-PC at 10 °C (10 mM phosphate buffer, pH 7.0). The fluorescence of Trp 59 (excited at 295 nm and detected above 310 nm) was measured in stopped-flow experiments (dead time ~ 1.7 ms), after equal volumes of protein and lipid in aqueous buffer solutions were mixed. The relative fluorescence was normalized to the initial fluorescence of unfolded apocyt *c* in the absence of lipid. (A) Traces (100 s) shown on a logarithmic time-scale, and (B) linear time-scale representation of the first 10 ms of the kinetic traces in panel A. Final protein concentration was 10 μM. Final concentrations of L-PC were as follows: 100 μM (1), 200 μM (2), 500 μM (3), 1 mM (4), 2 mM (5), and 5 mM (6). For each experiment eight kinetic traces were averaged. The lines represent least-squares fits to the experimental data with a minimum number of exponential terms (see Table 1).

the total amplitude but drops to 8% at 2 mM L-PC and becomes negligible at 5 mM lipid (Table 1). (C) A slow phase (> 1 s) has a rate and amplitude strongly dependent on protein concentration (4% of the total fluorescence change at 2 μM apocyt *c* increasing to 33% at 20 μM apocyt *c* for 500 μM L-PC; see Table 2). All kinetic phases are associated with an increase in fluorescence, consistent with the transfer of Trp 59 from the hydrophilic environment in the unfolded state of apocyt *c* in solution to a more hydrophobic surrounding upon folding and insertion into the lipid micelle (see below).

CD Folding Kinetics of Apocyt c in Lipid Micelles. Far-UV stopped-flow CD experiments allow a direct measure of formation of α-helical structure. Representative stopped-flow CD kinetic traces for the folding of apocyt *c* induced by the interaction with zwitterionic (L-PC) and negatively charged (L-PG) lipid micelles are shown in Figure 4. The folding reaction was monitored by the changes in ellipticity at 225 nm over a time scale up to 2 s and compared to the ellipticity values of unfolded apocyt *c* (U) and native cyt *c* (N) in solution (Figure 4A,B). The experimental traces were found to fit to one or two exponential phases, and a summary of rates and amplitudes for various lipid concentrations is presented in Table 3. The extent of folding, measured as the fraction of folded protein, *f* (see Table 3), correlates well with the level of α-helix determined from the equilibrium far-UV CD measurements (Figure 1, inset). Panel C shows the normalized kinetics as a fraction of unfolded protein defined as $[\theta_N - \theta_F(t)]/\theta_N$, in which θ_N is the value of the ellipticity of native cyt *c* in solution and $\theta_F(t)$ is the folded fraction of apocyt *c* as measured by the ellipticity at 225 nm at time *t*.

It is apparent from Figure 4 that the folding of apocyt *c* induced by L-PG micelles was almost complete within the dead time of the instrument (Figure 4B), while with L-PC the expected CD changes were almost completely detected (Figure 4A). The double-exponential fits for the folding kinetics of apocyt *c* in the zwitterionic lysolipid, L-PC, extrapolate to the level of unfolded apocyt *c* in solution (Figure 2A,C). In contrast, for the folding of apocyt *c* induced by the negatively charged L-PG lipid, only at lipid concentrations below the CMC (288 μM, see ref *13*) did the calculated fits extrapolate to the initial level of the unfolded protein (Figure 2B). At higher L-PG concentrations (above the CMC) a large fraction of the expected change occurs during the dead time of the stopped-flow CD instrument (1.7 ± 0.3 ms), and only ~20% of the total expected ellipticity change is captured in the first 5 ms (Figure 2B).

The stopped-flow CD folding kinetics is described by two phases with rates and amplitudes depending on lipid concentration (Table 3). The fast phase (k_1) occurs in less than 2−13 ms and the amplitude (a_1) associated with this phase accounts for the largest fraction of the total changes in ellipticity, varying from 67% for 200 μM L-PC to nearly 100% for 5 mM L-PC. The slower phase (k_2) occurs over 70−370 ms and becomes negligible for concentrations above 1 mM L-PC.

Binding and Insertion Kinetics. Vesicles labeled with FPE have been shown to provide valuable information on the kinetics of binding and insertion of charged peptides and protein into lipid membranes (*29*−*31*). We have incorporated the FPE probe into L-PC and L-PG micelles to characterize the kinetics of binding and insertion of apocyt *c* into these micelles and establish their correlation with kinetic phases detected by stopped-flow Trp 59 fluorescence and far-UV CD. Typical stopped-flow fluorescence kinetics of binding and insertion monitored by FPE is shown in Figure 5 for the interaction of apocyt *c* with L-PC micelles. The initial increase in fluorescence is associated with the binding of the polypeptide to the membrane surface, and the later phase of decreasing fluorescence represents the insertion of the polypeptide into the hydrophobic core of the lipid membrane (*29*). For both lipids, both the binding and insertion processes were found to fit double-exponential curves; i.e., the binding and insertion events were found to be biphasic processes.

Table 1: Fluorescence Kinetic Parameters for the Folding of Apocyt *c* Induced by L-PC for Various Lipid Concentrations[a]

[L-PC] (μM)	k_1 (s^{-1})	a_1	k_2 (s^{-1})	a_2	k_3 (s^{-1})	a_3	b[b]
100	80 (5)[c]	−0.034 (1)	6.6 (6)	−0.013 (1)	*d*	*d*	1.05
200	93 (5)	−0.049 (2)	16.3 (7)	−0.052 (1)	0.507 (9)	−0.0436 (3)	1.13
500	107 (4)	−0.100 (2)	19.9 (6)	−0.084 (3)	0.180 (3)	−0.0519 (3)	1.21
1000	128 (3)	−0.100 (3)	25.7 (9)	−0.077 (3)	0.28 (3)	−0.0077 (3)	1.22
2000	188 (3)	−0.223 (2)	26.9 (2)	−0.019 (2)	*d*	*d*	1.23
5000	379 (8)	−0.196 (4)	*d*	*d*	*d*	*d*	1.23

[a] Rate constants (k_i) and normalized amplitudes (a_i) to the initial fluorescence value of apocyt *c*, measured in the absence of lipid, were determined from stopped-flow Trp 59 fluorescence measurements at 10 °C for a final apocyt *c* concentration of 10 μM and various concentrations of L-PC. [b] End point. [c] Errors in the least significant digit (one standard deviation) are shown in parentheses. [d] Phase not observed.

Table 2: Fluorescence Kinetic Parameters for the Folding of Apocyt *c* Induced by L-PC for Various Protein Concentrations[a]

[apocyt *c*] (μM)	k_1 (s^{-1})	a_1	k_2 (s^{-1})	a_2	k_3 (s^{-1})	a_3	b[b]
2	228 (17)[c]	−0.035 (1)	42.7 (6)	−0.073 (1)	0.37 (2)	−0.005 (1)	1.13
5	203 (8)	−0.066 (1)	33.1 (6)	−0.104 (1)	0.44 (3)	−0.012 (1)	1.20
10	198 (4)	−0.116 (7)	26.7 (2)	−0.116 (1)	0.45 (4)	−0.042 (2)	1.27
15	318 (8)	−0.109 (1)	35.1 (3)	−0.109 (1)	0.95 (5)	−0.077 (1)	1.27
20	321 (9)	−0.106 (3)	34.0 (5)	−0.087 (1)	1.55 (8)	−0.087 (1)	1.26
5	159 (5)	−0.123 (3)	39.9 (1)	−0.064 (3)	*d*	*d*	1.25
10	103 (1)	−0.175 (1)	11.3 (3)	−0.0391 (7)	0.122 (6)	−0.0108 (2)	1.32
15	105 (1)	−0.149 (1)	14.1 (4)	−0.0424 (9)	0.294 (4)	−0.0391 (2)	1.30
20	103 (1)	−0.139 (1)	10.0 (3)	−0.0393 (7)	0.371 (4)	−0.0612 (3)	1.32
25	144 (3)	−0.106 (1)	23.9 (6)	−0.0543 (9)	1.24 (2)	−0.0571 (5)	1.30
30	143 (2)	−0.116 (1)	17.7 (6)	−0.0473 (7)	1.27 (4)	−0.0503 (8)	1.29

[a] Rate constants (k_i) and normalized amplitudes (a_i) to the initial fluorescence value of apocyt *c*, measured in the absence of lipid, were determined from stopped-flow Trp 59 fluorescence measurements at 10 °C for various concentrations of apocyt *c*, and L-PC concentrations of 500 μM (upper half of the Table) and 1 mM (lower half of the Table). [b] End point. [c] Errors in the least significant digit (one standard deviation) are shown in parentheses. [d] Phase not observed.

Biphasic behavior for both binding and insertion has been observed before for the interaction of peptides and proteins with FPE-labeled lipid vesicles (*30*, *32*).

The FPE kinetic results for the binding and insertion of apocyt *c* to L-PC micelles can be summarized as follows: (A) a very fast binding phase occurring within the first 2 ms, with a rate and amplitude dependent on lipid and protein concentrations; (B) a slow binding phase occurring in 10−30 ms, with a rate and amplitude dependent on lipid and protein concentrations; (C) a fast insertion phase happening in 200 ms−2 s, with rate and amplitude independent of lipid concentration, and (D) a last slow phase up to 40 s, with a rate and amplitude depending on protein concentration. The fast binding phase (process A) carries the largest change in fluorescence (>70% of the total fluorescence change). The dependence of phases A and B on lipid and protein concentrations indicate that these phases are associated with the second-order binding process of apocyt *c* to the lipid micelle. The rate of the second phase of increasing fluorescence (process B) has a strong dependence on protein concentration (this rate increases from 32 to 104 s^{-1} for 2 and 10 μM apocyt *c*, respectively, for a constant lipid concentration of 2 mM L-PC). Thus, this phase is likely to be associated with structural rearrangements of the protein on the micelle surface coupled with binding. In summary, the binding of apocyt *c* to L-PC micelles occurs in 2−30 ms, followed by insertion on a time scale from 200 ms to seconds, depending on protein concentration.

DISCUSSION

Structural Properties of Apocyt c in L-PC Micelles. When the heme group in cyt *c* is removed, the resulting protein, apocyt *c*, loses the properties of the well-folded compact structure characteristic of native cyt *c* (Figure 1). The resulting heme-free polypeptide chain has instead a largely unstructured conformation in solution (Figure 1; see also refs *7* and *8*). This indicates that the presence of the covalently bound heme group is an essential factor in determining the compact folded structure of native cyt *c*. However, we and others have shown that the binding of apocyt *c* to lipid membranes (in the absence of the heme group) induces a transition from a random coil conformation in solution to an α-helical structure (*11*, *13*). The extent of folding of apocyt *c* was shown to be lipid-dependent and can reach a level of α-helix content approaching that of native cyt *c* (*13*).

In the current study we report on the structure and folding kinetic properties of apocyt *c* induced by zwitterionic lipid micelles of L-PC in comparison with the folding of apocyt *c* induced by the interaction with negatively charged micelles of L-PG (*25*). As in the case of other membrane models, binding of apocyt *c* to L-PC micelles also induces the formation of α-helical structure (Figure 1). The amount of lipid-induced α-helix increases with lipid concentration and reaches a maximum value for concentrations above 1 mM lipid (Figure 1, inset). In contrast with negatively charged lipid micelles (*13*, *25*), which induce nearly 100% of the α-helix content of native cyt *c*, the maximum amount of α-helix induced by L-PC micelles is around 65% of that of cyt *c*. It is important to note that the comparison with the α-helical structure of cyt *c* refers only to the amount of α-helix, and it is not possible to infer from the current CD results whether the helices in the lipid-induced partially folded state of apocyt *c* involve the same segments of the polypeptide chain as in cyt *c*. However, a study by Jordi et

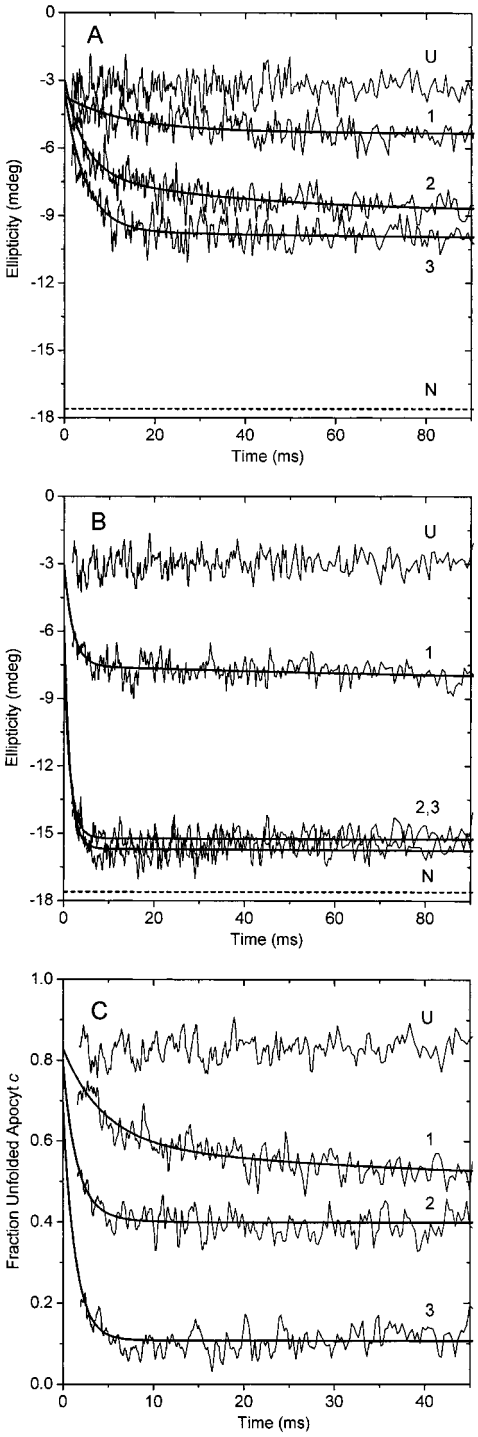

FIGURE 4: Representative far-UV CD kinetic traces for the folding of apocyt *c* at 10 °C induced by the interaction with L-PC and L-PG at various lipid concentrations. (A) L-PC: 200 μM (1); 1 mM (2); and 5 mM (3). (B) L-PG: 100 μM (1); 1 mM (2); and 5 mM (3). Panel C shows the normalized kinetics as a fraction of unfolded apocyt *c* measured as $[\theta_N - \theta_F(t)]/\theta_N$ (see text) for the folding of apocyt *c* induced by 1 mM L-PC (1) and by 100 μM (2) and 5 mM (3) L-PG. The ellipticity at 225 nm was measured in stopped-flow experiments (dead time ~ 1.7 ms) after equal volumes of protein and lipid in 10 mM phosphate buffer at pH 7.0 were mixed. Final protein concentration was 10 μM. The kinetic traces are compared with the ellipticity levels of the unfolded state of apocyt *c* (U) and native state of cyt *c* (N) in solution in the absence of lipid measured in control experiments in which protein was mixed with buffer. Traces are an average of 32 recordings, and the curves are single- or double-exponential least-squares fits to the experimental data points (see Table 3).

Table 3: Far-UV CD Kinetic Parameters for the Folding of Apocyt *c* Induced by Lipid Micelles[a]

lipid	[lipid] (μM)	k_1 (s^{-1})	a_1	k_2 (s^{-1})	a_2	$\theta_F - \theta_U$[b]	f[c]
L-PC	200	77 (9)[d]	1.47 (7)	2.7 (6)	0.72 (5)	2.9	0.34
L-PC	500	78 (7)	2.31 (9)	5 (2)	0.62 (8)	4.5	0.42
L-PC	1000	227 (22)	4.1 (2)	27 (3)	1.7 (2)	5.8	0.50
L-PC	2000	220 (21)	6.1 (5)	14 (7)	0.4 (1)	7.0	0.57
L-PC	5000	>500	6.9 (2)	*e*	*e*	7.6	0.60
L-PG	100	>500	4.5 (7)	6.3 (6)	1.00 (3)	5.7	0.49
L-PG	1000	>600	8 (1)	0.5 (5)	0.7 (5)	13.1	0.90
L-PG	2000	>700	10 (3)	1.1 (3)	0.8 (1)	13.7	0.94

[a] Rate constants (k_i) and amplitudes (a_i) were measured from stopped-flow CD folding kinetic experiments at 10 °C by monitoring the changes in the far-UV signal at 225 nm after rapid mixing of apocyt *c* with lipid (see Materials and Methods). [b] Expected total amplitude measured as the difference between the final ellipticity value of lipid-induced folded apocyt *c* (θ_F) at $t = 2$ s and the initial ellipticity value of the unfolded state (θ_U). [c] Fraction of folded protein measured as θ_F/θ_N, where θ_N is the ellipticity of native cyt *c*. [d] Errors in the least significant digit (one standard deviation) are shown in parentheses. [e] Phase not observed.

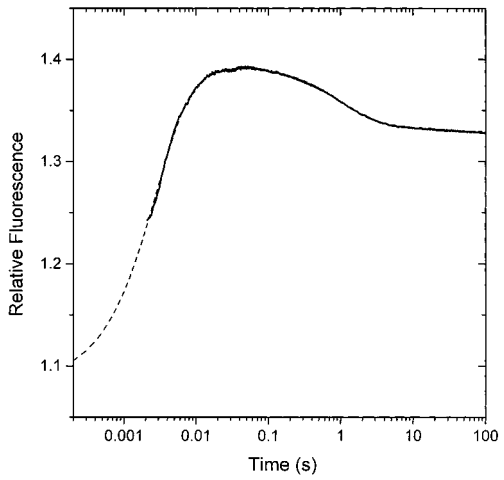

FIGURE 5: Typical binding and insertion kinetics monitored by FPE for the interaction of apocyt *c* with L-PC micelles at 10 °C. The fluorescence of FPE (excited at 490 nm and detected above 515 nm) was measured in stopped-flow measurements (dead time ~ 1.7 ms) after equal volumes of protein and FPE-labeled micelles were mixed (see Experimental Procedures) in 10 mM phosphate buffer, pH 7.0. The relative fluorescence was normalized to the initial fluorescence level of FPE-labeled micelles in the absence of protein. The trace (continuous line) is an average of four recordings for 2 mM L-PC with 10 μM apocyt *c*. The increase in fluorescence from 0 to 30 ms represents the binding of apocyt *c* to the micelle surface (see text), and the later decrease in fluorescence from ~100 ms to several seconds is ascribed to membrane insertion. The broken line represents a four-exponential least-squares fit to the experimental curve.

al. (*10*) on fragments of apocyt *c* suggests that the helices formed in apocyt *c* upon binding to lipid membranes are likely to correspond to the helices in the native protein, but detailed structural studies are required to resolve this issue.

The highly helical state of apocyt *c* in negatively charged L-PG micelles shows no stable tertiary structure, as revealed by the absence of signal in near-UV CD spectra (*25*). Likewise, the helical state of apocyt *c* in L-PC micelles shows no CD signal in the near-UV region (data not shown), which indicates that there are no specific packing interactions involving aromatic side chains. Therefore, this helical state in L-PC micelles also lacks stable tertiary structure. In

addition, results from energy transfer measurements with AEDANS-apocyt *c* (data not shown) show that the average Trp−AEDANS distance of the unfolded state was pH-dependent. At pH 2.0 the protein is a more extended random coil (average Trp−AEDANS distance around 27 ± 2 Å) than at pH 7.0 (Trp−AEDANS distance ∼21 ± 1 Å), in good agreement with a previous study (*25*). The lipid-bound states formed with 100 μM and 5 mM L-PC showed an average Trp−AEDANS distance around 21 ± 1 Å. These findings imply that the helical conformation in L-PC micelles is not a very compact state and is likely to be a highly dynamic state, at least at the level of the tertiary structure.

Kinetic Folding Mechanism of Apocyt c Induced by Lipid Micelles. We have shown that the kinetic folding mechanism of apocyt *c* induced by negatively charged lipid micelles proceeds via a collapsed intermediate state prior to insertion into the lipid phase (*25*). This lipid-induced folding process appears to be driven by electrostatic interactions between negatively charged lipid headgroups and the net positive charge of the protein, which induces the hydrophobic collapse of the polypeptide chain. Electrostatic lipid−protein interactions were thought to be the main driving force underlying the folding of apocyt *c* by lipid membranes (*11, 12*). However, we have shown that hydrophobic lipid−protein interactions play an important role in the lipid-induced folding of apocyt *c* (*13*). In the current study, we have investigated the folding kinetics of apocyt *c* induced by zwitterionic lipid micelles of L-PC, in comparison with the kinetic mechanism for the folding of apocyt *c* in L-PG micelles (*25*). In contrast with the folding of apocyt *c* induced by L-PG, the folding of apocyt *c* by L-PC micelles is predominantly driven by hydrophobic lipid−protein interactions.

Our Trp 59 stopped-flow fluorescence results show evidence for three main kinetic events: (A) a fast phase occurring in the range of 3−12 ms, depending on lipid concentration [the amplitude associated with this phase carries a large fraction of the total fluorescence change (34% for 200 μM L-PC increasing to nearly 100% for 5 mM L-PC)]; (B) an intermediate phase between 20 and 150 ms; and (C) a slow phase on a time scale larger than 1 s. The fast and intermediate phases are associated with the largest changes in fluorescence (together these phases carry 75 to 100% of the total fluorescence change), while the slow phase accounts only for a small fraction of the total fluorescence change (Tables 1 and 2). The fact that the slow phase has significant amplitude only at low lipid concentration and high concentrations of protein suggests that this is a second-order process, occurring under conditions where micelle concentration is smaller than or comparable to the concentration of apocyt *c*. The observation that k_3 depends strongly on protein concentration (Table 2) also indicates that this phase is probably due to binding of two or more protein molecules per micelle under conditions where [apocyt *c*] > [micelle]. The slow phase may thus reflect the dissociation of apocyt *c* from a transient aggregated state. This complication is largely avoided at [L-PC] > 1 mM (Table 1) or [apocyt *c*] < 10 μM (Table 2), where micelles are in excess over protein. In these limits where [micelle] > [apocyt *c*], a pseudo-first-order regime is reached and the kinetics is dominated by fast exponential processes. Therefore, processes A and B with the largest fluorescence changes are likely to correspond to the main protein folding events associated with lipid binding and insertion.

The stopped-flow FPE kinetics showed that binding of apocyt *c* to the surface of the lipid micelle occurs in the first few milliseconds (2−30 ms) and insertion phases were observed from 200 ms to several seconds, depending on protein concentration. Thus the fast phase (process A) detected by Trp fluorescence (3−12 ms) corresponds to the binding of apocyt *c* to the micelle surface, and the slow phase (process C; >1 s) is associated with the insertion of the protein into the hydrophobic core of the lipid micelle. The far-UV CD kinetic results showed that a large fraction of the α-helical structure is formed in the first few milliseconds (75−100% α-helix formed in <2−13 ms for L-PC and 80−95% α-helix formed in <2 ms for L-PG; see Table 3). This main kinetic phase in the stopped-flow CD kinetics corresponds to the fast phase detected by Trp fluorescence and overlaps with the binding phases observed by FPE kinetics.

Scheme 1

$$U_W \Leftrightarrow I_C \Leftrightarrow I_S \Leftrightarrow H_L$$

Scheme 2

$$U_W \Leftrightarrow I_S \Leftrightarrow H_L$$

On the basis of our combined kinetic results of stopped-flow Trp and FPE fluorescence with stopped-flow far-UV CD, we discuss two possible schemes for the kinetic folding mechanism of apocyt *c* in zwitterionic L-PC micelles (Schemes 1 and 2). In these schemes, U_W represents the initial unfolded state in aqueous solution and H_L represents the final helical state in lipid micelles. According to the equilibrium CD properties, the initial unfolded U_W state has a largely unstructured random coil conformation, and the final lipid-inserted helical state (H_L) has an α-helix content of about 65% of the helical structure of cyt *c* in solution (Figure 1, inset). In analogy with the folding mechanism of apocyt *c* induced by L-PG (*25*), the unfolded state may fold via a collapsed state (I_C) and a surface-associated intermediate (I_S) prior to insertion into the micelle (formation of H_L). Alternatively, the protein may bind to the micelle surface in a more extended conformation (I_S) followed by insertion into the micelle ($I_S \rightarrow H_L$) (Scheme 2). The involvement of a collapsed state I_C (as in Scheme 1) in the kinetic folding mechanism of apocyt *c* induced by L-PG was detected as a burst phase in the fluorescence-detected kinetics during the dead time of stopped-flow measurements (<2 ms) and was associated with the interaction of apocyt *c* with monomeric lipid molecules (*25*). By contrast, the kinetic results for the folding of apocyt *c* induced by L-PC micelles show no burst phase (Figure 3B). The formation of a collapsed state determines the amplitude of fluorescence changes associated with the subsequent kinetic phases. In contrast to the folding of apocyt *c* induced by L-PG micelles, where only a small fraction of the expected fluorescence change was detected (*25*), the kinetic amplitude associated with binding of apocyt *c* to L-PC micelles accounts for the total expected fluorescence change (Figure 3). Moreover, formation of I_C was associated with a burst increase in fluorescence during the dead time of the stopped-flow measurement, corresponding to the kinetic step $U_W \rightarrow I_C$ in Scheme 1, and the first

observed kinetic phase (above the CMC) was associated with a decrease in fluorescence. This phase was connected to the partial unfolding step, $I_C \rightarrow I_S$ (Scheme 1), and the observed decrease in fluorescence was consistent with transfer of Trp 59 from the hydrophobic core of I_C to a solvent-exposed location in the extended intermediate I_S associated with the micelle surface. In the current folding kinetics of apocyt *c* induced by L-PC micelles all phases are associated with an increase in fluorescence.

Occurrence of collapsed states during protein refolding in solution are generally associated with substantial folding, primarily at the level of secondary structure (*33*−*35*). Stopped-flow CD kinetic results show that rapid mixing of apocyt *c* with L-PG, both below and above the CMC, induced rapid formation of an α-helical state within the first few milliseconds (Figure 4B,C; Table 3). This early intermediate, associated with I_C, was found to be highly helical with 80−95% of the α-helix content of H_L, depending on lipid concentration. In contrast, the CD-detected folding kinetics of apocyt *c* induced by zwitterionic L-PC micelles occurs on the time scale of 2−13 ms, depending on lipid concentration (Table 3), and accounts for 75−100% of the expected CD signal changes monitored at 225 nm (Table 3). The first phase in the CD-detected kinetics is remarkably consistent with the time scale of the first kinetic step detected by tryptophan fluorescence ($1/k_1 \sim 3-12$ ms), and the second CD-detected phase (70−370 ms, depending on [L-PC]) partly overlaps with k_2 for Trp kinetics ($1/k_2 \sim 20-150$ ms) (see Tables 1 and 3). In addition, the kinetic results with FPE-labeled micelles show that binding occurs over the time scale 2−30 ms and insertion from 0.2 s to several seconds (Figure 5). The final level of FPE fluorescence (at 10 s; Figure 5) suggests that only a fraction of the polypeptide inserts into the hydrophobic core of the micelle. This interpretation is consistent with previous studies by Jordi et al. (*10*, *36*), in which it was shown that the N- and C-terminal helices insert into lipid membranes. Also, a recent study by polarized attenuated total reflection Fourier transform infrared spectroscopy (ATR FTIR) of apocyt *c* in lipid membranes (Bryson et al., unpublished results) revealed that the helical domains of apocyt *c* in lipid membranes have a net orientation perpendicular to the membrane, which is compatible with a partial lipid-inserted conformation of apocyt *c*. It is important to note that the insertion events monitored by the FPE probe (kinetic phases of decreasing fluorescence) are typically associated with a movement of the polypeptide from the membrane surface to a deeper location in the lipid membrane, which may or may not coincide with a transmembrane topology of the inserted α-helix (*29*−*32*). Thus it is unclear from the current FPE results whether the membrane-inserted α-helices of apocyt *c* adopt a fully transmembrane topology (i.e., helix axis normal to the membrane surface), and other experimental approaches are underway to resolve this issue.

The combined kinetic results of Trp and FPE fluorescence with far-UV CD kinetics provide strong support for the kinetic mechanism represented in Scheme 2, in which the folding of apocyt *c* induced by L-PC micelles involves the formation of an α-helical surface-associated intermediate concurrent with binding ($U_S \rightarrow I_S$) and followed by insertion into the micelle ($I_S \rightarrow H_L$). I_S accumulates under conditions where [apocyt *c*] > [micelle], due to protein−protein interactions on the micelle surface; otherwise, lipid insertion (formation of H_L) follows rapidly the appearance of I_S, and the kinetics detected by fluorescence and CD approaches a single-exponential phase at higher lipid concentrations (Tables 1 and 3, [L-PC] = 5 mM).

We have shown that the formation of α-helical structure of apocyt *c* occurs at the membrane surface, concomitant with the binding of the polypeptide to the membrane, and precedes membrane insertion. Formation of α-helix prior to membrane insertion has been predicted on thermodynamic grounds by White and Wimley (*37*), who have shown that formation of secondary structure in lipid interfaces is more favorable compared with the high energy cost of inserting free peptide bonds into lipid membranes. To our knowledge, here we have presented the first experimental demonstration of this prediction. Further, the kinetic folding mechanism of apocyt *c* driven by negatively charged lipid micelles of L-PG was found to involve a collapsed intermediate state (I_C) prior to insertion (*25*). In contrast, the folding of apocyt *c* induced by zwitterionic L-PC micelles (predominantly driven by hydrophobic lipid−protein interactions) does not involve the compact intermediate state I_C. Instead, the protein appears to bind to the micelle surface in a more extended conformation ($U_W \rightarrow I_S$), and this is followed by lipid insertion ($I_S \rightarrow H_L$). The initial binding step is concurrent with formation of a large fraction (75−100%, depending on lipid concentration) of the α-helical structure of the final lipid-inserted state H_L. The surface-associated helical intermediate (I_S) is formed on the time scale of 2−13 ms, depending on lipid concentration, and this is followed by insertion into the lipid micelle (formation of H_L) in the range of ∼200 ms to >1 s, depending on the lipid-to-protein ratio. I_S accumulates under conditions where [apocyt *c*] > [micelle], leading to protein−protein interactions on the surface of the lipid micelle and resulting in more complex kinetics due to dissociation of transient aggregated protein on the micelle surface. The final lipid-inserted helical state H_L in L-PC micelles has an α-helix content ∼65% of that of cyt *c* in solution and has no compact stable tertiary structure, as revealed by circular dichroism results. According to Trp−AEDANS energy transfer, this final lipid-inserted state is as extended as the unfolded state in solution at pH 7 and is likely to be a very dynamic state.

Biological Implications. In the cell, the biogenesis of cyt *c* starts with the synthesis of the precursor protein, apocyt *c*, in free cytoplasmic ribosomes, without the heme group or a cleavable amino-terminal signal sequence. Unlike most other mitochondrial precursor proteins, the import of apocyt *c* does not require ATP or a membrane potential, nor the mitochondrial protein import machinery (*1*). Instead, apocyt *c* appears to insert spontaneously and partially cross the outer mitochondrial membrane (*2*, *3*). Therefore, it is possible that the import pathway of apocyt *c* into mitochondria might involve partially folded intermediate states associated with the lipid membrane. Studies of the interaction of signal sequence peptides with phospholipid membranes have shown that if the peptide does not form an α-helical structure, it cannot insert into the lipid membrane (*38*). Thus, lipid-associated partially folded states of apocyt *c* may play a role in the *in vivo* mechanism of mitochondrial import, i.e., membrane insertion and translocation. These states may also be required for heme binding during the biogenesis of cyt *c* and may represent biologically significant states in the in vivo folding mechanism of cyt *c*.

ACKNOWLEDGMENT

We are grateful to Dr. A. Rodger (Department of Chemistry, University of Warwick) for the access to a fluorometer and maintenance of the CD spectropolarimeter, and Professor H. Roder (Fox Chase Cancer Center, Philadelphia, PA) for a critical reading of an early version of the manuscript and helpful suggestions. T.J.T.P. thanks Drs. D. Gregson and P. King (Applied Photophysics, Leatherhead, U.K.) for their support.

REFERENCES

1. Stuart, R. A., and Neupert, W. (1990) *Biochimie 72*, 115−121.
2. Hartl, F. U., and Neupert, W. (1990) *Science 247*, 930−938.
3. Glick, B., and Schatz, G. (1991) *Annu. Rev. Genet. 25*, 21−44.
4. Hennig, B., and Neupert, W. (1981) *Eur. J. Biochem. 121*, 5241−5247.
5. Pfanner, N., Hartl, F.-U., and Neupert, W. (1987) *Eur. J. Biochem. 175*, 205−212.
6. Liu, X., Kim, C. N., Yang, J., Jemmerson, R., and Wang, X. (1996) *Cell 86*, 147−157.
7. Stellwagen, E., Rysavy, R., and Babul, G. (1972) *J. Biol. Chem. 247*, 8074−8077.
8. Fisher, W. R., Taniuchi, H., and Anfinsen, C. B. (1973) *J. Biol. Chem. 248*, 3188−3195.
9. Kuroda, Y. (1993) *Biochemistry 32*, 1219−1224.
10. Jordi, W., Li-Xin, Z., Pilon, M., Demel, R. A., and de Kruijff, B. (1989) *J. Biol. Chem. 264*, 2292−2301.
11. De Jongh, H. H. J., and de Kruijff, B. (1990) *Biochim. Biophys. Acta 1029*, 105−112.
12. Pinheiro, T. J. T., Elöve, G. A., Roder, H., de Jongh, H. H. J., de Kruijff, B., and Watts, A. (1995) in *Perspectives on Protein Engineering and Complementary Technologies*, Vol. 3, pp 62−65, Mayflower Worldwide, Oxford, U.K.
13. Rankin, S. E., Watts A., and Pinheiro, T. J. T. (1998) *Biochemistry 37*, 12588−12595.
14. Kranz, R., Lill, R., Goldman, B., Bonnard, G., and Merchant, S. (1998) *Mol. Microbiol. 29*, 383−396.
15. Roder, H., Elöve, G. A., and Englander, S. W. (1988) *Nature 335*, 700−704.
16. Elöve, G. A., Chaffotte, A. F., Roder, H., and Goldberg, M. E. (1992) *Biochemistry 31*, 6876−6883.
17. Elöve, G. A., Bhuyan, A. K., and Roder, H. (1994) *Biochemistry 33*, 6925−6935.
18. Sauder, J. M., and Roder, H. (1998) *Folding Des. 3*, 293−301.
19. Brautigan, D. L., Ferguson-Miller, S., and Margoliash, E. (1978) *Methods Enzymol. 53*, 128−164.
20. Margoliash, E., and Walasek, O. F. (1967) *Methods Enzymol. 10*, 339−348.
21. Hennig, B., and Neupert, W. (1983) *Methods Enzymol. 97*, 261−274.
22. Small, D. M. (1986) in *Physical Chemistry of Lipids. From Alkanes to Phospholipids* (Hanahan, D. J., Ed.) pp 58−72, Plenum Press, New York and London.
23. Hamada, D., Hoshino, M., Kataoka, M., Fink, A. L., and Goto, Y. (1993) *Biochemistry 32*, 10351−10358.
24. Hudson, E. N., and Weber, G. (1973) *Biochemistry 12*, 4154−4161.
25. Rankin, S. E., Watts, A., Roder, H., and Pinheiro, T. J. T. (1999) *Protein Sci. 8*, 381−393.
26. Colón, W., Elöve, G. A., Wakem, L. P., Sherman, F., and Roder, H. (1996) *Biochemistry 35*, 5538−5549.
27. Colón, W., and Roder, H. (1996) *Nat. Struct. Biol. 3*, 1019−1025.
28. Pinheiro, T. J. T., Elöve, G. A., Watts, A., and Roder, H. (1997) *Biochemistry 36*, 13122−13132.
29. Wall, J., Golding C. A., Van Veen, M., and O'Shea, P. (1995) *Mol. Membr. Biol. 12*, 183−192.
30. Golding, C., Senior, S., Wilson M. T., and O'Shea, P. (1996) *Biochemistry 35*, 10931−10937.
31. Cladera, J., and O'Shea, P. (1998) *Biophys. J.* 74, 2434−2442.
32. Wolfe, C., Cladera, J., and O'Shea, P. (1999) *Mol. Membr. Biol.* (in press).
33. Kim, P. S., and Baldwin, R. L. (1990) *Annu. Rev. Biochem. 59*, 631−660.
34. Matthews, C. R. (1993) *Annu. Rev. Biochem. 62*, 653−683.
35. Roder, H., and Colón, W. (1997) *Curr. Opin. Struct. Biol. 7*, 15−28.
36. Jordi, W., de Kruijff, B., and Marsh, D. (1989) *Biochemistry 28*, 8998−9005.
37. White, S. H., and Wimley, W. C. (1994) *Curr. Opin. Struct. Biol. 4*, 79−86.
38. Wang, Y., and Weiner, H. (1994) *Biochemistry 33*, 12860−12867.

BI990119O